The Astrophysical Journal Letters, 714:L41–L46, 2010 May 1 doi:10.1088/2041-8205/714/1/L41

FAST CONTRACTION OF CORONAL LOOPS AT THE FLARE PEAK

Rui Liu and Haimin Wang
Space Weather Research Laboratory, Center for Solar-Terrestrial Research, NJIT, Newark, NJ 07102, USA; rui.liu@njit.edu
Received 2010 January 31; accepted 2010 March 10; published 2010 April 1

ABSTRACT

On 2005 September 8, a coronal loop overlying the active region NOAA 10808 was observed in *TRACE* 171 Å to contract at ∼100 km s^{-1} at the peak of an X5.4–2B flare at 21:05 UT. Prior to the fast contraction, the loop underwent a much slower contraction at ∼6 km s^{-1} for about 8 minutes, initiating during the flare preheating phase. The sudden switch to fast contraction is presumably corresponding to the onset of the impulsive phase. The contraction resulted in the oscillation of a group of loops located below, with the period of about 10 minutes. Meanwhile, the contracting loop exhibited a similar oscillatory pattern superimposed on the dominant downward motion. We suggest that the fast contraction reflects a suddenly reduced magnetic pressure underneath due either to (1) the eruption of magnetic structures located at lower altitudes or to (2) the rapid conversion of magnetic free energy in the flare core region. Electrons accelerated in the shrinking trap formed by the contracting loop can theoretically contribute to a late-phase hard X-ray burst, which is associated with Type IV radio emission. To complement the X5.4 flare which was probably confined, a similar event observed in *SOHO*/EIT 195 Å on 2004 July 20 in an eruptive, M8.6 flare is briefly described, in which the contraction was followed by the expansion of the same loop leading up to a halo coronal mass ejection. These observations further substantiate the conjecture of coronal implosion and suggest coronal implosion as a new exciter mechanism for coronal loop oscillations.

Key words: Sun: corona – Sun: flares – Sun: oscillations – Sun: X-rays, gamma rays

Online-only material: color figures, animation

1. INTRODUCTION

Solar eruptions such as flares and coronal mass ejections (CMEs) are generally due to the disruption of the force balance between the upward magnetic pressure force, $-\nabla B^2/8\pi$, of a highly stressed field and the downward magnetic tension force, $(1/4\pi)(\mathbf{B}\cdot\nabla)\mathbf{B}$, of the overlying quasi-potential field. Since gravitational potential energy and thermal energy play no significant role in the corona, solar eruptions can only derive their energies from the free energy stored in the coronal magnetic field (e.g., Forbes 2000), which must decrease between the states before and after the eruption. The reduction of magnetic energy, $\int B^2/8\pi\, dV$, and hence of the average magnetic pressure, $B^2/8\pi$, would inevitably result in the contraction of the confining field so as to achieve a new force balance (Hudson 2000). Observations of coronal implosion, however, have been extremely rare.

Recently, Liu et al. (2009, hereafter Paper I) presented the contraction of the *Transition Region and Coronal Explorer* (*TRACE*) 171 Å and 195 Å coronal loops overlying the flaring region of a *GOES*-class C8.9 flare and an M7.6 flare, respectively. The contraction in both events was initiated during the flare preheating phase and sustained for about 10 minutes at an average speed of ∼5 km s^{-1}. Particularly, the former event was associated with the converging motion of the conjugate flare footpoints and the downward motion of a hard X-ray looptop source. Following the contraction, the same group of loops expanded outward, which eventually led to the eruption of the whole magnetic structure and a fast CME. The latter event was associated with the downward motion a looptop source in both *TRACE* 195 Å and hard X-rays.

Liu & Wang (2009, hereafter Paper II) studied the evolution of a group of *TRACE* 195 Å coronal loops overlying a reverse S-shaped filament. These loops were initially pushed upward with the filament ascending and kinking slowly, but after the filament rose explosively, they underwent contraction as fast as ∼100 km s^{-1}, sustaining for at least 12 minutes. We suggest that the escaping of the kinking filament results in the contraction of the overlying coronal loops, which can be regarded as a variant of coronal implosion. The contracting loops form a natural shrinking trap, which can efficiently accelerate electrons (Somov & Kosugi 1997). This may help to understand a single hard X-ray burst at the end of the contraction, which is characterized by nonthermal coronal emission distinctly above the post-flare arcade, with no corresponding rise in soft X-rays. Such flare late-phase bursts have been often attributed to the acceleration and trapping of electrons in the post-flare loop systems (e.g., Cliver et al. 1986) or to the acceleration of electrons in a shock front (e.g., Frost & Dennis 1971). The mechanism suggested in Paper II, however, involves a transfer of the free magnetic energy from the core field to the confining arcade during the eruptive process. The energy transferred is then made available to the trapped particles in the aftermath of the partial eruption, through the contraction of the overlying loops that have not reconnected.

Although it has been observed to occur preceding explosion (Paper I), as well as following explosion (Paper II), coronal implosion has not been reported during the flare impulsive phase or the CME rapid acceleration phase, as the original implosion idea predicts (Hudson 2000). Here, we present the fast contraction of an overlying coronal loop at the peak of a *GOES*-class X5.4 flare (the optical class 2B) observed by *TRACE* on 2005 September 8 in Section 2.1. A similar event in an M8.6 flare observed by the *SOHO* Extreme-ultraviolet Imaging Telescope (EIT) on 2004 July 20 is briefly described in Section 2.2. Concluding remarks are made in Section 3.

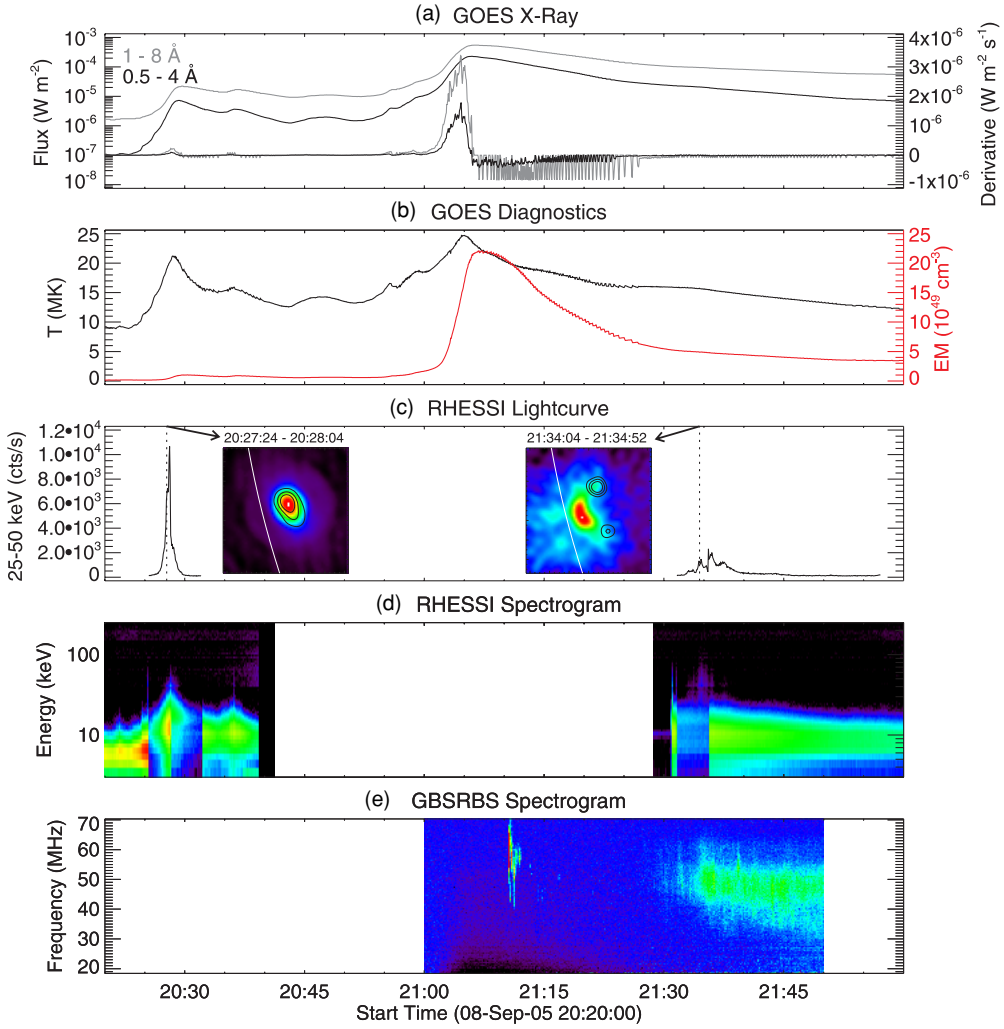

Figure 1. 2005 September 8 event observed by *GOES* and *RHESSI* as well as the ground-based Green Bank Solar Radio Burst Spectrometer (GBSRBS). The insets of panel (c) show *RHESSI* images synthesized by the CLEAN algorithm. The images are in the 12–25 keV energy range, overlaid by contours at 25–50 keV with contour levels at 30%, 50%, and 70% of the maximum brightness. Both thick and thin attenuators are in front of the detectors (A3 state) for both images.

(A color version of this figure is available in the online journal.)

2. OBSERVATION AND DATA ANALYSIS

2.1. X5.4 Flare on 2005 September 8

The X5.4 flare peaked in soft X-ray flux at about 21:06 UT on 2005 September 8, preceded by an M2.1 flare in the same active region, AR 10808 (S12E83), at about 20:30 UT (Figure 1(a)). *RHESSI* had coverage for the M2.1 flare, but unfortunately missed the impulsive and major phases of the X5.4 flare when it passed by the South Atlantic Anomaly region from 20:40 to 20:57 UT and then went into eclipse until 21:30 UT. Only a late-phase hard X-ray burst was recorded at about 21:35 UT (Figures 1(c) and (d)). It is unclear whether this X-class flare resulted in a CME: no *SOHO* data are available for the day of 2005 September 8; the Mark IV coronameter at Mauna Loa Solar Observatory (MLSO) only produced images from 18:17 till 20:08 UT. However, no mass ejection was observed in the ground-based He I (λ = 10830 Å, provided by MLSO) or Hα (λ = 6563 Å, provided by MLSO and Big Bear Solar Observatory) data. Similarly, no eruption was observed by the Solar X-Ray Imager (SXI) on board *GOES*. Small jets were indeed seen by *TRACE* around the peak of the X5.4 flare (see the video accompanying Figure 2). It is unknown whether the jets went into interplanetary space due to *TRACE*'s limited field of view (FOV; 8.5 × 8.5 arcmin). Moreover, it is not associated with any strong radio burst, except Type IV emission at the late-phase hard X-ray burst (Figure 1(e)). The absence of a CME in such a major flare is rare (Sheeley et al. 1983; Yashiro et al. 2005), but not unprecedented (Feynman & Hundhausen 1994). Hence, we conclude that this is very likely a confined flare.

The contraction of the coronal loop overlying AR 10808 was again observed by *TRACE*, thanks to its high spatial resolution (∼1 arcsec) and high time cadence (∼40 s; see the video accompanying Figure 2; a more comprehensive movie can be found at the *TRACE* Web site[1]). In Figure 2(a), two slits, labeled 1 and 2, are placed across the contracting loop (labeled L_C) and a group of oscillating loops (labeled L_O), respectively. L_C is delineated in a dotted line in Figure 2(b), which was taken at the beginning of the fast contraction, and again in Figure 2(e), which was taken near the end of the contraction. The northern leg of L_C can be hardly seen, presumably behind L_O. L_C exhibited clear downward movement starting around 21:04:48 UT at a height of $\sim 10^{10}$ cm, until at least 21:27:55 UT at a height of $\sim 5 \times 10^9$ cm, from which there is a data gap until

[1] http://trace.lmsal.com/POD/movies/T171_20050908_20X5.mov

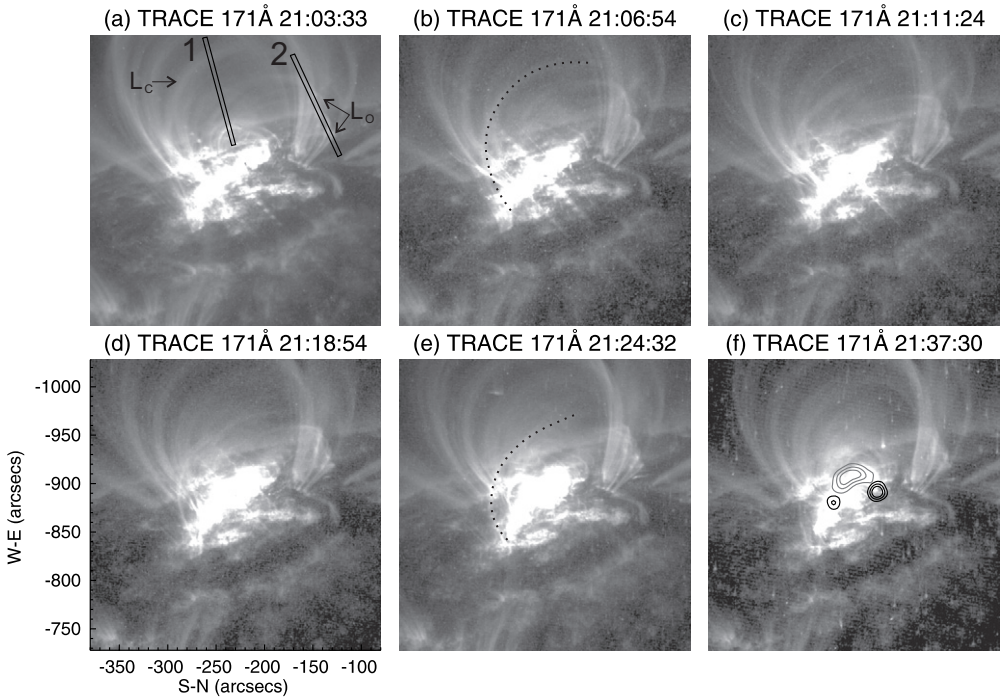

Figure 2. Snapshots of *TRACE* 171 Å images. Note that north is on the left and east is on the top. In frame (a), the loop that contracted inward is labeled L_C and the group of loops that oscillated when interacting with L_C is labeled L_O. Two slits, labeled 1 and 2, are placed across L_C and L_O, respectively. L_C is delineated in a dotted line in frames (b) and (e). Frame (f) is overlaid with *RHESSI* contours in the 12–25 keV (gray; brightness contour levels: 40%, 60%, and 80%) and 25–50 keV (black; brightness contour levels: 30%, 50%, and 70%) energy bands. Data accumulation for image synthesis using the CLEAN algorithm spans from 21:34:04 to 21:34:52 UT.
(An animation of this figure is available in the online journal.)

21:37:30 UT, when the loop top was hardly seen (Figure 2(f)), but the southern leg was still visible. The whole loop became invisible in the next available image at 21:40:05 UT, presumably overwhelmed by the core region with enhanced brightness. In Figure 2(f), the *TRACE* image is overlaid with *RHESSI* contours synthesized with the CLEAN algorithm. Data accumulation for image synthesis spans from 21:34:04 to 21:34:52 UT to cover the late-phase hard X-ray burst. The flare emission in the 12–25 energy range takes the form of a loop (brightness contour levels: 40%, 60%, and 80%), whose endpoints are roughly cospatial with the pair of conjugate footpoints at 25–50 keV (brightness contour levels: 30%, 50%, and 70%). In contrast, for the M2.1 flare at 20:30 UT, the emission in the same two energy bands is cospatial (see the insets of Figure 1(c)).

Figures 3(e) and (f) show the same *TRACE* image as Figure 2(a). We have applied the difference of two Gaussian filters with different "radii" (standard deviations) to the image to enhance the features of interest, whose size depends on the difference between the two radius values. The slices of *TRACE* images cut by the slits are then rotated to a vertical direction and placed on the time axis in Figures 3(a)–(d). During the flare preheating phase, the soft X-ray flux increased gradually from about 20:53 UT onward (see Figure 1(a)), and L_C was observed to contract very slowly at an average speed of $\sim$6 km s^{-1}, starting as early as 20:57 UT till 21:05 UT, when it suddenly switched to fast contraction at 117 km s^{-1} (Figures 3(a) and (b)). L_C then interacted with a group of loops, L_O (see Figure 2(a)), and resulted in their oscillation with the period of about 10 minutes (see Figures 3(c) and (d)). The speed of contraction decreased each time L_C was "pushed" back by L_O, first down to $\sim$50 km s^{-1} and then eventually down to $\sim$5 km s^{-1}. Due to this interaction, the contracting loop also exhibited a similar oscillatory pattern, but less obvious, since it was superimposed on the dominant downward motion (see Figures 3(a) and (b) and the video accompanying Figure 2). Meanwhile, the oscillation was damped quickly, consistent with the statistics of *TRACE* observations that $t_D/P = 4.0 \pm 1.8$ (Aschwanden 2003), where t_D is the damping time and P is the oscillation period. Prior to the fast contraction of L_C, two loops below L_C can be seen to rise upward from 20:58 till 21:05 UT, at a speed of $\sim$64 km s^{-1} and $\sim$16 km s^{-1}, respectively, with the lower one rising faster (see Figures 3(a) and (b)). Both rising loops became too diffused to be tracked, however, with L_C starting to contract fast. It is unclear whether they erupted eventually, since most loops located higher than L_C remained intact.

Two mechanisms could result in the reduction of the magnetic pressure underneath L_C and the consequent contraction. First, the supposed eruption of the two lower loops that was observed to rise upward prior to L_C's fast contraction (see Figure 3(b) and the video accompanying Figure 2). This mechanism is similar to the one proposed in Paper II, in which magnetic pressure decreased due to the escaping of a kinking filament underlying the loop that underwent contraction subsequently. Second, the rapid conversion of the magnetic free energy in the core field into radiative and thermal energies. In that case, the contraction of the overlying loop is a direct response to the reduced magnetic pressure at much lower altitudes where the energy conversion is ongoing. Since pressure pulses propagate at Alfvén speed in a magnetized plasma, there should be a time delay between the onset of the flare impulsive phase and that of the fast loop contraction.

Based on the derivatives of *GOES* soft X-ray fluxes (Figure 3(g)), which usually resemble the hard X-ray profile due to the Neupert effect (Neupert 1968), one can see that the impulsive phase started at 21:01:30 UT and peaked at 21:04:30 UT. Hence the fast contraction, which started at

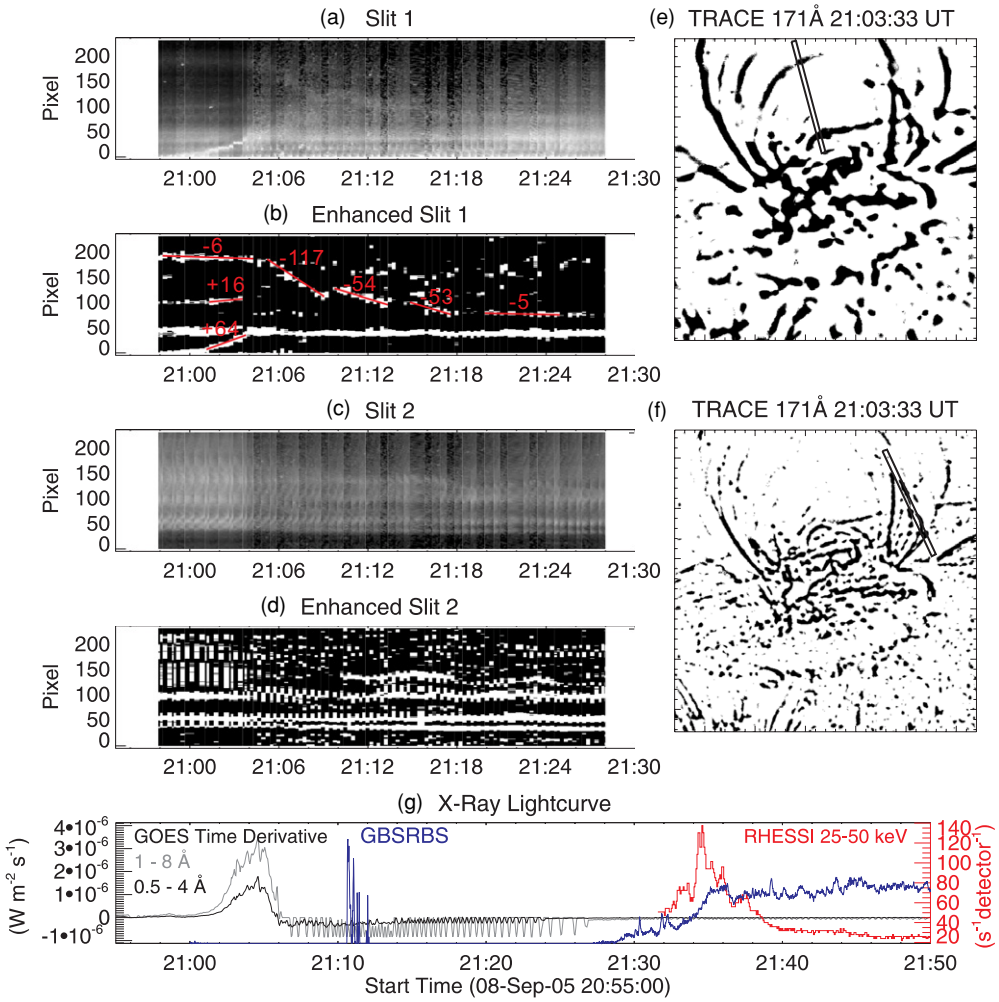

Figure 3. Series of *TRACE* images cut by slits. Original *TRACE* images cut by slits 1 and 2 are rotated to a vertical direction and placed on the time axis in (a) and (c), respectively. Corresponding enhanced *TRACE* images cut by the slits are placed in (b) and (d), respectively. In panels (e) and (f), the *TRACE* image is enhanced using the IDL procedure, EDGE_DOG, with different parameters being chosen to enhance features of different sizes (see the text for details). Slits 1 and 2 as labeled in Figure 2(a) are shown in (e) and (f), respectively. Panel (g) shows time derivatives of *GOES* soft X-ray fluxes and *RHESSI* count rates corrected approximately for the effects of attenuator and decimation state changes. The summed lightcurve of GBSRBS spectra is plotted in blue in an arbitrary unit.

(A color version of this figure is available in the online journal.)

21:04:48 UT, is delayed by about 200 s relative to the beginning of rapid magnetic energy conversion. Consistently, the slow contraction starting from 20:57 UT is delayed relative to the beginning of the preheating phase (20:53 UT) by the similar duration. The delay corresponds to an average speed, $v \simeq 10^{10}\,\mathrm{cm}/200\,\mathrm{s} = 500\,\mathrm{km\,s^{-1}}$, presumably the average speed of the Alfvén wave ($V_A = 2.18 \times 10^{11} B/\sqrt{n}$ cm s^{-1}) in the lower corona, where B could vary from 1 to 10^2 G and n from 10^8 to 10^{11} cm^{-3} in terms of order of magnitude.

The loop oscillation may provide additional diagnostic on the Alfvén speed. Observed as the transverse displacement of the loop position, it is most likely a fast kink mode oscillation. Moreover, for oscillations with the period of 10 minutes, fast kink mode has the highest probability for EUV loops observed in *TRACE* 171 Å (see Figure 7 in Aschwanden et al. 1999). The period of the fast kink mode can be approximated as follows (Roberts et al. 1984):

$$P \approx \frac{2L}{jV_A},$$

where L is the full loop length and j determines the number ($= j - 1$) of nodes in the oscillation along the loop. The loop half length for the group of oscillatory loops, L_O, is roughly measured to be 50 Mm. Thus, for the fundamental harmonic number ($j = 1$),

$$V_A \approx \frac{2L}{P} \simeq \frac{2 \times 10^5\ \mathrm{km}}{600\ \mathrm{s}} \simeq 300\ \mathrm{km\ s^{-1}},$$

which is comparable with the average Alfvén speed inferred above.

The Type IV emission (see Figure 1(e)) associated with the late-phase hard X-ray burst is often interpreted as plasma radiation from electrons trapped in large magnetic loops (Dulk 1985). Following Paper II, for electrons trapped in a shrinking loop, the parallel momentum increases due to longitudinal adiabatic invariant, $P_\parallel(t)h(t)$, i.e., $P_\parallel(t_1)/P_\parallel(t_0) = h(t_0)/h(t_1) \approx 10^{10}\,\mathrm{cm}/5 \times 10^9\,\mathrm{cm} = 2$, and the perpendicular momentum increases due to transversal adiabatic invariant, $P_\perp^2(t)/B$. We estimate the field at the loop top by an empirical formula for the coronal magnetic field of active regions (Dulk & McLean 1978), namely, $B(t_0) \simeq 0.5(h(t_0)/R_\odot)^{-3/2} \simeq 9$ G and $B(t_1) \simeq 0.5(h(t_1)/R_\odot)^{-3/2} \simeq 26$ G, hence $P_\perp(t) \xrightarrow{t \to t_1} 1.7 P_\perp(t_0)$

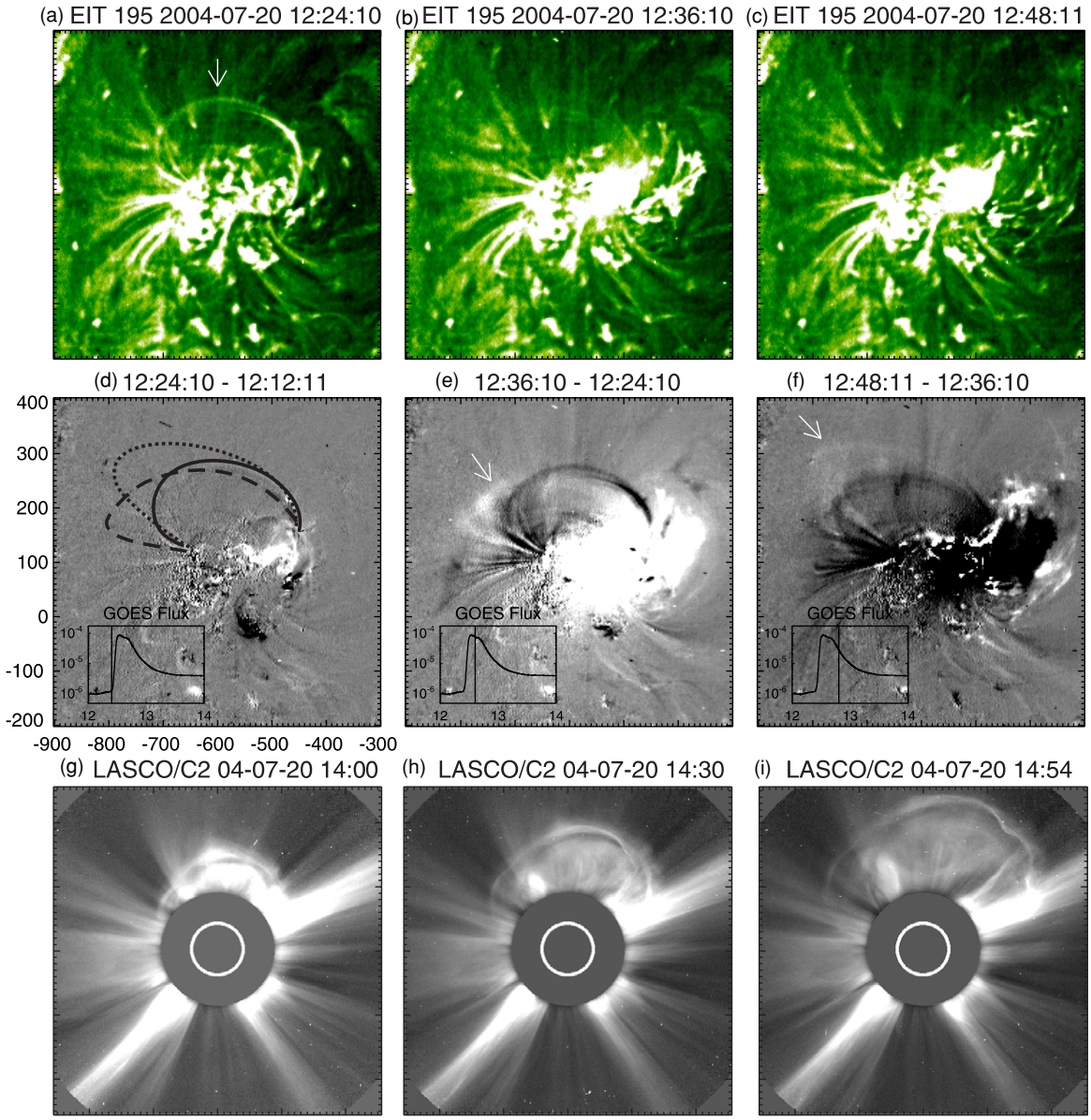

Figure 4. M8.6 flare observed with *SOHO*/EIT 195 Å. The top row shows the EIT images enhanced with a wavelet technique based on Stenborg & Cobelli (2003), and the middle row shows the corresponding running difference images with the insets displaying *GOES* 1–8 Å fluxes (W m^{-2}). The vertical line in each inset indicates the time when the corresponding EIT image was taken. The overlying loop that underwent contraction followed by expansion is marked by arrows. In panel (d), the loop at three different times is delineated in a solid line, a dashed line, and a dotted line, respectively. The bottom panels show white-light higher corona observed by the *SOHO* Large Angle and Spectrometric Coronagraph (LASCO).

(A color version of this figure is available in the online journal.)

and $E_k(t) = (P_\perp(t)^2 + P_\parallel(t)^2)/2m_e \xrightarrow{t\to t_1} 7E_k(t_0)$. Despite that some energy was dissipated through the loop oscillation, hot electrons of several keV could be accelerated to nonthermal energy range in this trap (see also Paper II), therefore contributing to the hard X-ray burst observed at the end of implosion (21:32–21:38 UT). Similar to the late-phase hard X-ray burst reported in Paper II, there is absence of the Neupert effect (Figure 1(a)), and the looptop source is significantly hardened ($\gamma \simeq 3$) relative to the footpoints ($\gamma \simeq 5$), based on an imaging spectroscopic analysis.

2.2. M8.6 Flare on 2004 July 20

The *GOES*-class M8.6 flare occurred in the active region NOAA 10652 (N05E32) at about 12:30 UT on 2004 July 20. Figure 4 shows three consecutive EIT 195 Å images (the top row) as well as the corresponding running difference images (the middle row) at the onset of the flare (Figures 4(a) and (d)), near the flare peak (Figures 4(b) and (e)), and during the gradual phase of the flare (Figures 4(c) and (f)), respectively. Despite the relatively poor time cadence (12 minutes), one can see that the overlying coronal loop (marked by arrows) was pushed downward during the flare impulsive phase, ending up with a flat top very similar to the loop L_C in Figure 2. Most extraordinarily, the loop was then stretched upward, eventually leading up to a halo CME (see the bottom panels of Figure 4), with the CME front bearing similarity with the loop of interest. If the loop indeed evolved into the CME front, then there is no preceding eruption that could result in the observed contraction, as the first mechanism in Section 2.1 suggests. Therefore, this observation

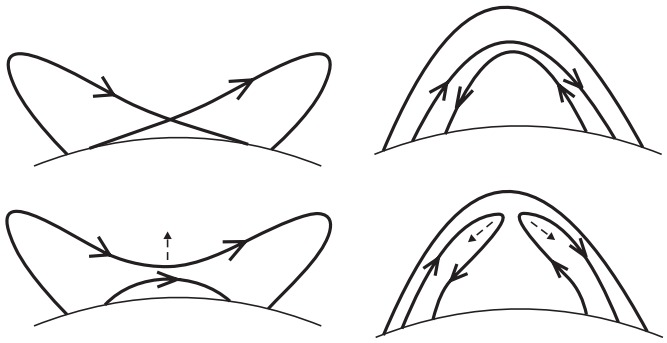

Figure 5. Sketch of magnetic reconnections in different scenarios with implications for the possibility of coronal implosion. Left column: the two-dimensional adaptation of the tether-cutting reconnection as proposed in Moore et al. (2001); right column: reconnection between an emerging magnetic field and the existing field of the opposite polarity. Solid arrows indicate the direction of the magnetic field line and dashed arrows the direction of the magnetic tension force.

is in favor of the second mechanism, namely, the contraction as a direct consequence of the rapid energy conversion process in the flare core region.

3. DISCUSSION AND CONCLUSION

To summarize, we focus on the contraction of a *TRACE* 171 Å coronal loop overlying the X5.4 flare region on 2005 September 8. The observation features a two-stage evolution of contraction, which started with a slow speed at ~6 km s^{-1} for about 8 minutes, and then suddenly switched to a much faster speed as high as 117 km s^{-1}, corresponding to the onset of the flare impulsive phase. During the latter stage, the contracting loop interacted with a group of loops located below and drove their oscillation. Due to this interaction, the contracting loop also exhibited a similar oscillatory pattern superimposed on the dominant downward motion. The fast contraction presumably reflects a suddenly reduced magnetic pressure underneath due either to (1) the eruption of magnetic structures located at lower altitudes or to (2) the rapid conversion of magnetic free energy in the flare core region. Owing to the lack of CME signatures in this event, the interpretation of the late-phase hard X-ray event and Type IV emission in terms of a shrinking trap (also see Paper II) is favored over the competing mechanisms, which require a Type II burst (Frost & Dennis 1971) or magnetic reconnection following CMEs (Cliver et al. 1986), respectively. In addition, our observation demonstrates that magnetic implosion can excite coronal loop oscillations, which, however, has been generally believed to be driven by outward-pushing waves in a flare or a filament destabilization (e.g., Schrijver et al. 2002).

The observations of loop contraction initiating during the flare preheating phase in Paper I, during the impulsive phase in this paper, and during the gradual phase in the wake of a filament eruption in Paper II have substantiated the conjecture of coronal implosion (Hudson 2000) and implied its occurrence in general conditions. Although only the loops with the "right" temperature and density are visible in a narrow EUV filter, it can be reasonably assumed that the whole relevant magnetic structure is undergoing contraction, with magnetic loops at higher altitudes contracting at later times, dependent on the local Alfvén speed. In that sense, implosion indeed occurs simultaneously with the energy release in the flaring region, in agreement with Hudson's idea that implosion is neither the consequence nor the cause of the flare, but part of the flaring process.

The rarity of implosion events can be partly accounted for by the following observational constraints. First of all, high-resolution, high-cadence, and large-FOV observations are necessitated, but only the forthcoming Solar Dynamics Observatory can provide such a data set. Second, the contracting loop may fail to show up in a thin filter like *TRACE* 171 Å or 195 Å. Third, coronal loops are better observed above the limb, and their contraction is best observed when the line of sight is perpendicular to the loop plane. On the other hand, implosion may provide clues to the magnetic configuration involved in the eruption. For example, a tether-cutting reconnection would create a tension force pointing upward (see the left column of Figure 5), which can help balance the downward tension force imposed by the confining field; alternatively, reconnection between an emerging magnetic field and the existing field of the opposite polarity would yield tension forces pointing sideward and downward (see the right column of Figure 5), which makes implosion possible.

The authors are thankful to the anonymous referee for helpful comments. We acknowledge the *TRACE*, *RHESSI,* and *SOHO* consortia for the excellent data. R.L. thanks Chang Liu for help on data analysis. This work was supported by NASA grant NNX08-AJ23G and NNX08-AQ90G, and by NSF grant ATM-0849453.

REFERENCES

Aschwanden, M. J. 2003, in Turbulence, Waves, and Instabilities in the Solar Plasma, ed. R. Erdélyi, K. Petrovay, B. Roberts, & M. J. Aschwanden (Dordrecht: Kluwer), 215
Aschwanden, M. J., Fletcher, L., Schrijver, C. J., & Alexander, D. 1999, ApJ, 520, 880
Cliver, E. W., et al. 1986, ApJ, 305, 920
Dulk, G. A. 1985, ARA&A, 23, 169
Dulk, G. A., & McLean, D. J. 1978, Sol. Phys., 57, 279
Feynman, J., & Hundhausen, A. J. 1994, J. Geophys. Res., 99, 8451
Forbes, T. G. 2000, J. Geophys. Res., 105, 23153
Frost, K. J., & Dennis, B. R. 1971, ApJ, 165, 655
Hudson, H. S. 2000, ApJ, 531, L75
Liu, R., & Wang, H. 2009, ApJ, 703, L23 (Paper II)
Liu, R., Wang, H., & Alexander, D. 2009, ApJ, 696, 121 (Paper I)
Moore, R. L., Sterling, A. C., Hudson, H. S., & Lemen, J. R. 2001, ApJ, 552, 833
Neupert, W. M. 1968, ApJ, 153, L59
Roberts, B., Edwin, P. M., & Benz, A. O. 1984, ApJ, 279, 857
Schrijver, C. J., Aschwanden, M. J., & Title, A. M. 2002, Sol. Phys., 206, 69
Sheeley, N. R., Jr., Howard, R. A., Koomen, M. J., & Michels, D. J. 1983, ApJ, 272, 349
Somov, B. V., & Kosugi, T. 1997, ApJ, 485, 859
Stenborg, G., & Cobelli, P. J. 2003, A&A, 398, 1185
Yashiro, S., Gopalswamy, N., Akiyama, S., Michalek, G., & Howard, R. A. 2005, J. Geophys. Res. (Space Phys.), 110, 12